Structure and acidity of Mo/H-MCM-22 catalysts studied by NMR spectroscopy

Shing-Jong Huang[a], Qi Zhao[a,b], Wen-Hua Chen[a], Xiuwen Han[b], Xinhe Bao[b], Pang-Shuen Lo[c], Huang-Kuei Lee[c], Shang-Bin Liu[a,*]

[a]*Institute of Atomic and Molecular Sciences, Academia Sinica, P.O. Box 23-166, Taipei 106, Taiwan, ROC*
[b]*Dalian Institute of Chemical Physics, Chinese Academy of Sciences, Dalian, PR China*
[c]*Institute of Materials Science and Manufacturing, Chinese Culture University, Taipei 111, Taiwan, ROC*

Abstract

A comprehensive study on physical and chemical properties of Mo/MCM-22 bifunctional catalysts has been made by using combined analytic and spectroscopic techniques, such as adsorption, elemental analysis, and ^{129}Xe and ^{31}P NMR of adsorbed trialkylphosphine oxide probe molecules. Samples prepared by the impregnation method with Mo loadings ranging from 2–10 wt.% have been examined and the results are compared with that obtained from samples prepared by mechanical mixing using MoO_3 or Mo_2C as agents. Sample calcination treatment is essential in achieving a well-dispersed metal species in Mo/MCM-22. It was found that, upon initial incorporation, the Mo species tend to inactivate both Brønsted and Lewis sites locate predominantly in the supercages rather than the 10-membered ring channels of MCM-22. However, as the Mo loading exceeds 6 wt.%, the excessive Mo species tend to migrate toward extracrystalline surfaces of the catalyst. A consistent decrease in concentrations of acid sites with increasing Mo loading <6 wt.% was found, especially for those with higher acid strengths. Upon loading of Mo > 6 wt.%, further decreases in both Brønsted and Lewis acidities were observed. These results provide crucial supports for interpreting the peculiar behaviors previously observed during the conversion of methane to benzene over Mo/MCM-22 catalyst under non-oxidative conditions, in which an optimal performance was achieved with a Mo loading of 6 wt.%. The effects of Mo incorporation on porosity and acidity features of the catalyst are discussed.
© 2004 Published by Elsevier B.V.

Keywords: Mo/MCM-22; Bifunctional catalyst; NMR; Porosity; Acidity.

1. Introduction

Bifunctional catalysts, such as transition metal incorporated zeolites, are known to promote direct conversion of methane to benzene and toluene under non-oxidative conditions [1-4]. Among them, the dehydroaromatization reaction has received intense attention due to energy-related issues [3]. In an earlier study, Bao and co-workers [4] revealed that Mo incorporated zeolites with a Mo loading of ca. 2–10 wt.% are suitable bifunctional catalysts for the methane dehydroaromatization reaction. The authors also concluded that, in terms of catalytic performance, the Mo/H-MCM-22 catalyst is far superior to Mo/H-ZSM-5. In particular, an optimal performance of the Mo/H-MCM-22 catalyst was found with a Mo loading of ca. 6 wt.%, by which a high benzene selectivity (80%) with depressed naphthalene yield and prolonged catalyst life can be achieved with a moderate methane conversion of 10%. The authors hypothesized that the outstanding catalytic performance is mainly due to the unique pore structure possessed by the MCM-22 zeolite [5]. In this context, the effects of incorporated Mo on the pore structure and acid site distribution of MCM-22 deserves further investigation.

The structure of MCM-22 zeolite consists of two independent two-dimensional pore systems; namely, the sinusoidal channels with 10-MR openings and the larger 12-MR supercages (0.71 nm × 0.71 nm × 1.81 nm) interconnected

* Corresponding author. Tel.: +886 2 23668230; fax: +886 2 23620200.
E-mail address: sliu@sinica.edu.tw (S.-B. Liu).

by the 10-MR windows [6]. Owing to its extraordinarily large extracrystalline surface area compared to its zeolite counterparts, MCM-22 is more favorable in catalyzing reactions that predominantly occur on the external surface of the catalyst.

Owing to its chemical inertness, high polarizability and wide range of chemical shift (>5000 ppm), ^{129}Xe NMR [7,8] spectroscopy of adsorbed xenon is sensitive to its local environments and hence has been widely used for porosity characterization. As a result, numerous applications in porous materials, such as zeolites and molecular sieves, can be found [9,10]. Such a technique has also been utilized by Chen et al. to investigate the pore structure of MCM-22 [11]. The authors concluded that, at moderate loading, xenon molecules tend to adsorb preferentially in the supercages and due to the high degree of tortuosity in MCM-22, xenon can diffuse into the sinusoidal 10 MR channels only when the Xe pressure exceeds ca. 6 atm. Nevertheless, samples with nearly saturated loading of Xe were used in their variable-temperature study, indicating that the predominant chemical shift contribution is due to Xe–Xe interactions. The aforementioned report thus lacks information on Xe-zeolite wall interactions, which can be obtained either directly by adopting a sample with dilute Xe loading or by extrapolating the ^{129}Xe NMR chemical shift versus Xe loading curve to zero loading. For the latter, preparation of samples with different Xe loading pressures is essential.

A novel solid-state ^{31}P MAS-NMR technique developed recently reveals the potency in simultaneous determination of the types and strengths of acid sites in solid acid catalysts using trimethylphosphine (TMP) [12-15] or trimethylphosphine oxide [16-18] as probes. From the viewpoint of NMR applications, since the ^{31}P nucleus possesses a higher sensitivity and a wider chemical shift range (>300 ppm) compared to ^{13}C and ^{15}N, thus these phosphorus molecules are advantageous over other conventional NMR probes, such as pyridine or methyl amine [19,20]. In a recent study, we went further to demonstrate that such a ^{31}P NMR technique, when applied with a proper choice of trialkylphosphine oxides as probe molecules and in conjunction with elemental analysis by ICP-MS, is capable of providing quantitative information on internal and external acid sites [21]. The discernment of internal versus external acid sites is made possible by using phosphorus probe molecules with varied kinetic diameters, for example, for 10-MR zeolites with an average pore aperture of ca. 0.6 nm, trimethylphosphine oxide (TMPO, size ca. 0.55 nm) and tributylphosphine oxide (TBPO, size ca. 0.82 nm) are suitable choices as probes. TMPO whose size is smaller than the pore aperture, can diffuse into the intracrystalline channels of the zeolites, thus providing concurrent detection of both the internal and external acid sites. TBPO whose size is too large to penetrate into the channels, can merely detect acid sites located on the extracrystalline surface of the zeolites. Accordingly, detailed acid features, viz. the types, strengths, concentration and

location of the acid sites, can be simultaneously determined [21].

The objective of this work is to investigate the effects of incorporated Mo on the pore structure and acid site distribution of Mo/H-MCM-22 catalysts. The variation in their pore characteristics is studied by room temperature (298 K) Xe adsorption isotherm measurements and variable-temperature ^{129}Xe NMR of adsorbed Xe. Variations in their acid properties are studied by ^{31}P MAS-NMR of adsorbed TMPO. Mo/H-MCM-22 catalysts with varied Mo loading prepared by different methods, namely impregnation and mechanical mixing, are examined.

2. Experimental

2.1. Materials

MCM-22 zeolite was synthesized by the procedure reported by Shu et al. [4]. Known amounts of sodium metaaluminate, sodium hydroxide (96% NaOH), hexamethyleneimine (HMI, about 85%), silica (95% SiO$_2$) and deionized water were mixed and vigorously agitated in a vessel for 30 min. The chemical composition of the mixture was as follows: SiO$_2$/Al$_2$O$_3$ = 30, OH$^-$/SiO$_2$ = 0.18, Na/SiO$_2$ = 0.18, HMI/SiO$_2$ = 0.32 and H$_2$O/SiO$_2$ = 43. The resultant gel was introduced into a stainless-steel autoclave, followed by heating to 423 K until complete crystallization occurred. After quenching the autoclave to room temperature, the solid sample was separated from the mixture by centrifugation at 5000 rpm, washed by deionized water then dried at 383 K overnight. The powder was then subjected to calcination in air at 853 K for 4 h to obtain the as-synthesized sample. The H-form MCM-22 zeolite was obtained by successive exchanging with NH$_4$NO$_3$ aqueous solution and calcination.

Mo/H-MCM-22 catalysts with varied Mo loading prepared by different methods, namely impregnation and physical mixing, are examined. The samples prepared by the impregnation method were done by introducing a desired amount of ammonium heptamolybdate (AHM) aqueous solution into the H-MCM-22 zeolite at 358 K for 16 h, followed by drying for 4 h at 393 K, then calcination in air at 853 K for 4 h. Accordingly, samples with different Mo loading, denoted as xMoOM22IC (x represents the amount of Mo introduced; x = 2-10 wt.%); the index 'IC' at the end stands for calcined sample preparation by the impregnation method. Two additional series of samples containing ca. 6 wt.% Mo were prepared by the mechanical mixing method, one by mixing a desired amount of MoO$_3$ with H-MCM-22 zeolite (denoted as 6MoOM22M), followed by calcination at 853 K for 4 h (denoted as 6MoOM22MC), the other one by mixing Mo$_2$C with H-MCM-22 (denoted as 6MoCM22M), followed by thermal treatment under a He gas stream at 923 K for 0.5 h (denoted as 6MoCM22MH). For the latter, Mo$_2$C compound was prepared by the method reported by Lee et al. [22].

2.2. Sample pretreatment and adsorption studies

Adsorption of xenon, 1,3,5-TMB and TMPO guest molecules are invoked in this study. Prior to each experiment, the sample was subjected to dehydration treatment by gradual heating to the desired temperature under vacuum ($<10^{-5}$ Torr) at 623 K for at least 24 h, except for Mo-loaded samples. To prevent possible redistribution of the Mo species, all Mo-loaded samples were dehydrated at 473 K. The weight of each sample was carefully monitored before and after the dehydration procedure.

Xenon adsorption isotherm measurements were carried out at room temperature (298 K) by the volumetric method. The detailed experimental setup and procedures can be found elsewhere [23,24]. To facilitate variable-temperature (VT) ^{129}Xe NMR experiments, a home-design NMR sample cell (Pyrex; 7 mm i.d.) with a pre-pulled neck at ca. 23 mm from the bottom was used [25]. The sample cell is attached to a vacuum stopcock and an adapter so that it can be conveniently set up for dehydration of the sample and subsequent adsorption of Xe on a vacuum apparatus. A known amount of Xe in a calibrated volume was transferred into the dehydrated sample contained in the designated NMR cell region whose exterior was immersed in a liquid N_2 bath, then the sample capsule was sealed off with a mini-torch. Special care was taken in minimizing the dead volume of each sample capsule during glass sealing. In the case of co-adsorption of 1,3,5-TMB (99%; Acros) and Xe, a certain amount 1,3,5-TMB (equivalent to the number of supercages in MCM-22) was first introduced into the dehydrated sample, followed by the Xe adsorption procedures described above.

Adsorption of TMPO is somewhat more cumbersome due to its bulk nature at ambient temperature. First, a desirable amount of TMPO (100% Alfa) was dissolved in CH_2Cl_2, then, the solution was introduced into a cell containing a dehydrated sample by a gastight syringe in a glovebox under N_2 atmosphere. The slurry sealed in the sample cell was placed into an ultrasonic bath for 30 min and then allowed to sit statically overnight. Subsequently, the solvent in the slurry was removed under vacuum, then the sealed sample cell was heated at 423 K for 3 h to ensure a uniform adsorption of TMPO in the porous adsorbent. Finally, the adsorbate-loaded sample was transferred into a ZrO_2 MAS-NMR rotor (4 mm o.d.) under an N_2 glovebox.

2.3. NMR experiments

Room temperature ^{129}Xe NMR experiments were performed on a Bruker MSL-300 NMR spectrometer, operating at a Larmor frequency of 83.012 MHz, whereas ^{13}C and VT-^{129}Xe NMR experiments were carried out on a Bruker MSL-500P NMR spectrometer, operating at 138.326 and 125.758 MHz using TMS and dilute Xe gas as chemical shift reference, respectively. All spectra obtained from NMR experiments were acquired by single-pulse sequence with a pulse-length of ca. $\pi/6$. Typically, 16,000 and 4000–20,000 free induction decay (FID) signals were accumulated using a recycle delay of 600 and 300 ms during ^{13}C and ^{129}Xe NMR experiments, respectively. The number of accumulations applied to each sample is to ensure that the resultant FIDs possess adequate sensitivity, which depends on adsorbate loading. Solid-state ^{31}P MAS-NMR experiments were performed on the Bruker MSL-500P spectrometer, corresponding to a resonance frequency of 202.46 MHz. A single-pulse sequence with a $\pi/6$ pulse and a recycle delay of 5 s was used. Typically, spectra were obtained by accumulation of 500–1000 FID signals under a sample spinning frequency of 10–12 kHz.

2.4. Elemental analysis

All samples loaded with TMPO were further subjected to elemental analysis by ICP (Jarrell-Ash, ICP 9000) to obtain elemental contents of Si, Al, P and Mo. This is done by dissolving each sample (ca. 0.1 g) in a HF, HCl and HNO_3 mixture (10 mL) followed by introducing ca. 60 mL of saturated boric acid solution at room temperature. Concentration of each element so obtained was determined using a commercial standard.
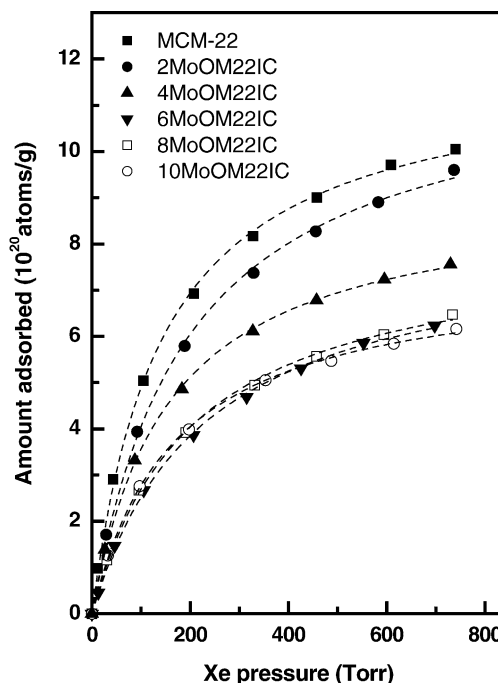

Fig. 1. Room-temperature (298 K) Xe adsorption isotherms of parent MCM-22 and various calcined *x*MoOM22IC samples (*x* = 2–10 wt.%) prepared by the impregnation method. The dashed lines represent non-linear fittings.

3. Results and discussion

3.1. Xenon adsorption and ^{129}Xe NMR

All room temperature Xe adsorption isotherms obtained from the parent and various Mo-loaded MCM-22 samples prepared by different methods reveal typical Langmuir-type adsorption curves, as shown in Figs. 1 and 2. Compared to the parent MCM-22, the Xe adsorption capacity of xMoOM22IC samples ($0 < x \leq 6$ wt.%; Fig. 1) gradually decreases with increasing Mo loading (x), indicating a gradual pore volume decrease in the presence of certain amounts of Mo species. However, the observed adsorption capacity reaches a plateau when $x \geq 6$ wt.%, suggesting that the surplus Mo species do not prefer to reside in the intracrystalline pores of MCM-22. On the other hand, the adsorption capacities and the effect of calcination (or thermal) treatment for various Mo-incorporated samples prepared by different methods may also be compared. As shown in Fig. 2, the Xe uptake in these samples at room temperature follows the trend: MCM-22 > 6MoOM22I > 6MoOM22M > 6MoOM22MC > 6MoCM22M > 6MoCM22MH > 6MoOM22IC. Thus, it is conclusive that, in terms of competency of incorporating Mo species into the intracrystalline voids of MCM-22: (1) a sample prepared by the impregnation method is superior to one prepared by mechanical mixing; (2) for samples prepared by mechanical mixing, those mixed with Mo_2C are better than those mixed with MoO_3; and (3) additional calcina-

tion or thermal treatment is essential to ensure migration of Mo species into pores of MCM-22.

Similar conclusions can be drawn based on the results obtained from room temperature ^{129}Xe NMR of adsorbed Xe, by which all spectra revealed only a single, symmetrical resonance peak whose chemical shift (ranging from 100–140 ppm; not shown) varies with Xe loading. The effect of Mo loading on variations of chemical shift versus Xe density curves can be deduced from Fig. 3. For a given sample with known Mo loading, the chemical shift curve reveals a typical upward parabolic characteristic, whose chemical shift values increases with increasing Xe concentration. The effect of different sample preparation methods and thermal post-treatments on variation of chemical shift can be inferred from Fig. 4. In general, the observed chemical shift in the low xenon loading (Henry's law) regime can be expressed by the following equation [7-9,23-27]:

$$\delta(r) = \delta_0 + \delta_s + \sigma_{Xe}\rho, \tag{1}$$

where δ and ρ denote chemical shift and xenon loading, respectively. The term δ_0 is the chemical shift reference (0 ppm). The term δ_s, which represents chemical shift at zero xenon loading ($\rho = 0$), reflects interaction between Xe and the pore surfaces of the adsorbent. Thus, the δ_s term can further be divided into two chemical shift contributions, namely those that arise from Xe-zeolite wall and Xe–Mo species interactions, whose value can easily be obtained by extrapolating the chemical shift line (at low
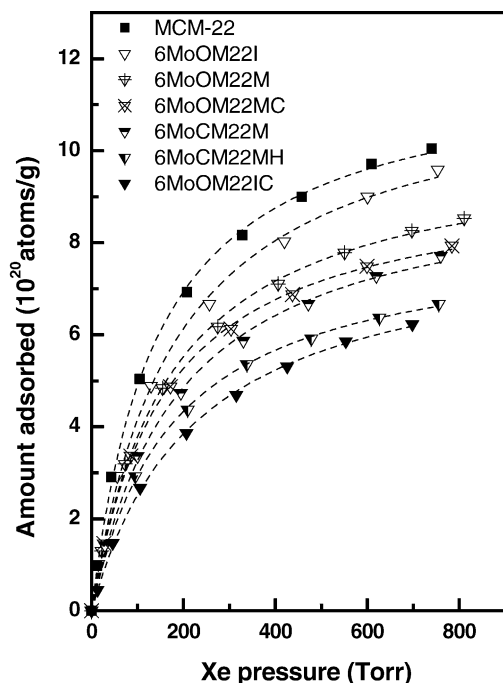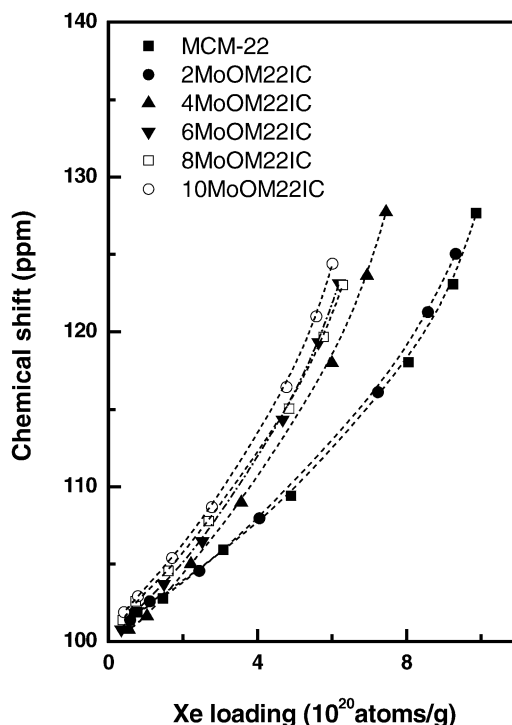

Fig. 2. Comparisons of Xe adsorption isotherms (298 K) for parent MCM-22 and various Mo/MCM-22 samples (with 6 wt.% Mo loading) prepared by different methods and thermal treatments (see text). The dashed lines represent non-linear fittings.

Fig. 3. Variations of ^{129}Xe chemical shift with Xe loading obtained (at 298 K) from parent MCM-22 and various calcined xMoOM22IC samples (x = 2–10 wt.%) prepared by the impregnation method. The dashed lines represent non-linear fittings.
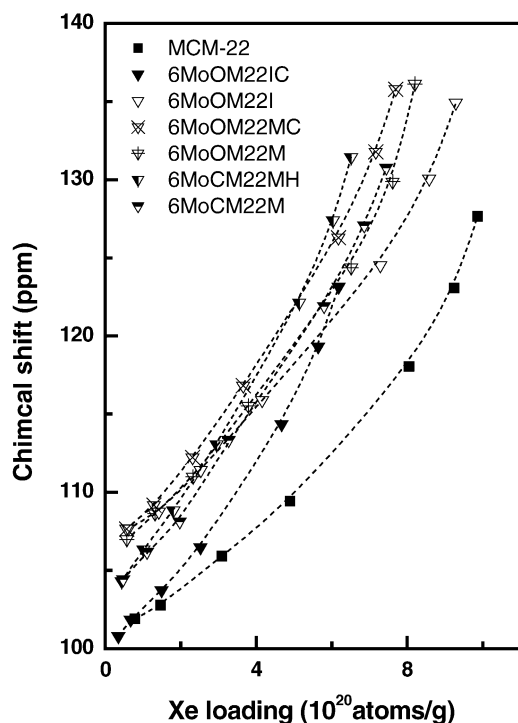
Fig. 4. Variations of [129]Xe chemical shift with Xe loading obtained (at 298 K) from parent MCM-22 and various Mo/MCM-22 samples (6 wt.% Mo loading) prepared by different methods and thermal treatments (see text). The dashed lines represent non-linear fittings.

Xe loading) to the chemical shift axis. On the other hand, the last term proportional to ρ is the characteristic of Xe–Xe interactions. Accordingly, related [129]Xe NMR parameters can be obtained by fitting the experimental data using Eq. (1), as depicted in Table 1.

It is evident that the δ_s value of Mo/MCM-22 samples reveals the expected gradual increase with increasing

Mo loading compared to parent MCM-22 (δ_s = 97.9). For calcined Mo/MCM-22 samples prepared by the impregnation method, a consistent increase in σ_{Xe} value from 2.47 to 3.34 with increasing Mo loading (x) from 0 to 6 wt.% was observed. Note that, while the δ_s value continues to increase with Mo loading, the σ_{Xe} value remains practically unchanged for $x \geq 6$ wt.%. It will be seen later that these observations are in complete agreement with the results obtained from Xe adsorption measurements.

3.2. VT-[129]Xe NMR studies

VT-[129]Xe NMR spectra obtained from various samples with a xenon density of 1.0 amagat (gas density at 273 K and 1 atm; i.e., $\rho = 2.704 \times 10^{19}$ atoms/cm^3 for Xe) are illustrated in Fig. 5. For parent MCM-22 the room temperature spectrum reveals a symmetrical peak at ca. 103 ppm. Upon lowering the temperature, the resonance splits into three peaks when $T < 220$ K, indicating three distinct pore environments in MCM-22. For example, three resonance peaks corresponding to chemical shifts of 102.3, 118.4 and 142.0 ppm can be resolved at 160 K. It is anticipated that these resonance arise from fast exchange of Xe among different pore environments. Similar behaviors were also observed for the 2MoOM22IC sample, as shown in Fig. 5b, for which three distinct resonances at 104.8, 118.4 and 144.5 ppm are evident at 160 K. Such phenomena, however, are not observed for the 6MoO-M22IC sample (Fig. 5c); a linewidth broadening occurs at temperature below 240 K at first, then becomes narrow again at $T < 200$ K. It can be seen later that this is mainly due to blockage of certain pore structures by the Mo species present in the sample. The assignments of [129]Xe NMR chemical shifts to different porous environments will be discussed in the following section.

Table 1
List of [129]Xe NMR parameters for various samples[a]

Preparation method	Sample	Mo loading (wt.%)	δ_s (ppm)	σ_{Xe} (ppm/atom g^{-1})	V/V_o (%)	λ (nm)
Parent	MCM-22	0	97.9	2.47	100.0	0.304
Impregnation[b]	2MoOM22IC	2	98.3	2.49	99.3	0.302
	4MoOM22IC	4	98.4	3.18	77.8	0.302
	6MoOM22IC	6	98.4	3.34	74.0	0.302
	8MoOM22IC	8	99.7	3.31	74.7	0.295
	10MoOM22IC	10	100.1	3.32	74.5	0.293
	6MoOM22I	6	105.4	2.58	95.7	0.268
Mechanical mixing with MoO$_3$	6MoOM22MC[c]	6	105.5	3.02	81.9	0.268
	6MoOM22M	6	104.7	2.80	88.3	0.271
Mechanical mixing with Mo$_2$C	6MoCM22MH[d]	6	102.6	3.15	78.5	0.281
	6MoCM22M	6	102.9	3.29	75.2	0.280

[a] Obtained from Eq. (1).

[b] Samples with different Mo loading (x), denoted as xMoOM22IC, index 'IC' stands for samples calcined in air at 853 K for 4 h.

[c] After calcination treatment.

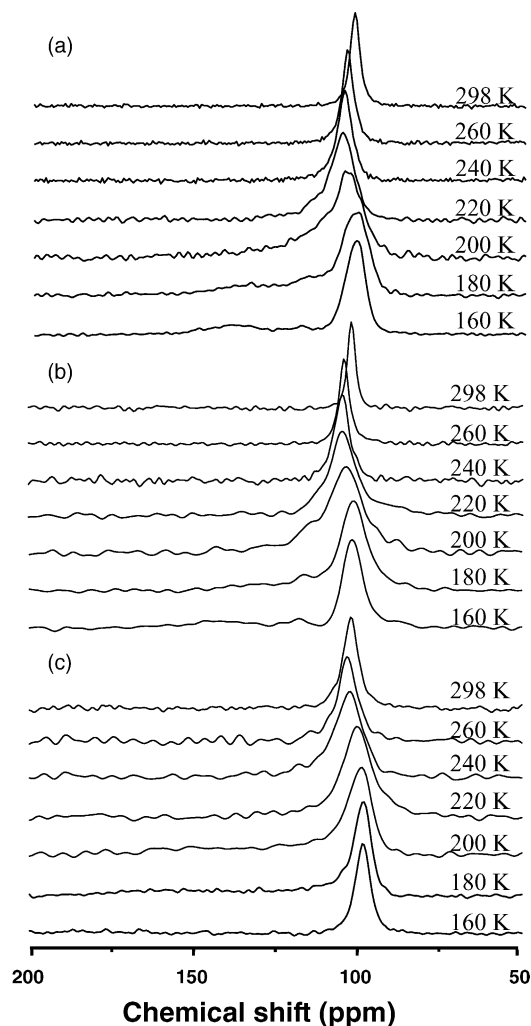[d] After thermal treatment under He gas stream at 923 K for 0.5 h.

Fig. 5. Variable-temperature ^{129}Xe NMR spectra of Xe (loading 1 amagat = 2.704×10^{19} atoms/cm^3) adsorbed on: (a) parent MCM-22; (b) 2MoO-M22IC; and (c) 6MoOM22IC samples.

3.3. Porous structure of MCM-22

For parent MCM-22, the observed δ_s value (97.9 ppm; Table 1) derived by Eq. (1) from the room temperature ^{129}Xe NMR results, can be correlated to the pore diameter of zeolites [23,26] as:

$$\delta_s = \frac{A}{B + \lambda} \tag{2}$$

where λ is the average free path of Xe (in nm), and $A = 49.9$ and $B = 0.2054$ are empirical constants. For zeolites with infinite long and straight cylindrical channels, λ can further be expressed by:

$$\lambda = D_{\text{Zeolite}} - D_{\text{Xe}} \tag{3}$$

where D_{Zeolite} and D_{Xe} denote the zeolite channel diameter and the Xe kinetic diameter (0.440 nm), respectively. Accordingly, a λ value of 0.304 nm (Table 1) for Xe can be determined by Eq. (2) and, consequently, an effective pore diameter of 0.744 nm can be derived for parent MCM-

22 by Eq. (3). As mentioned earlier, MCM-22 zeolite possesses two independent microporous systems [5,6], one the sinusoidal channels consisting of 10-MR, which have an average dimension of ca. 0.4 nm × 0.59 nm, and the other the larger supercages (0.71 nm × 0.71 nm × 1.81 nm) composed by 12-MR, which are interconnected by the 10-MR windows (0.4 nm × 0.54 nm). Obviously, the effective channel diameter so derived for parent MCM-22 is in good agreement with the average diameter of the supercages. Thus, it can be concluded that, although the adsorbed Xe in MCM-22 zeolite can undergo fast exchange between two different pore systems at room temperature, the resonance coalesces to produce a single, symmetrical line in the ^{129}Xe NMR spectrum and Xe atoms predominantly prefer to locate in the supercages (when the xenon loading is less than ca. 1.0 × 10^{21} atoms/g; Fig. 2) rather than in the 10-MR channels. The same conclusion has also been made by Chen et al. for a similar sample system, but with a much higher Xe loading [11].

Furthermore, the exchange rate of Xe adsorbed in MCM-22 is expected to slow down at lower temperature, which facilitates observation of individual ^{129}Xe NMR resonance arising from respective pore environments. In order to, clarify the origin of the three ^{129}Xe resonance signals observed on a parent MCM-22 sample at 160 K, additional ^{129}Xe NMR experiments were performed on a sample co-adsorbed with 1,3,5-TMB and Xe. This was done by first introducing an appropriate amount of 1,3,5-TMB, which is equivalent to the number of supercages, into the dehydrated MCM-22 sample followed by adsorption of Xe and ^{129}Xe NMR measurement. However, since the size of 1,3,5-TMB (ca. 0.7 nm) is comparable to the pore diameter of supercages in MCM-22, the ^{129}Xe NMR spectrum (Xe loading 1 amagat) obtained right after adsorption of 1,3,5-TMB (Fig. 6a), which is in close resemblance to that observed for parent MCM-22 (Fig. 5a), indicates the absence of
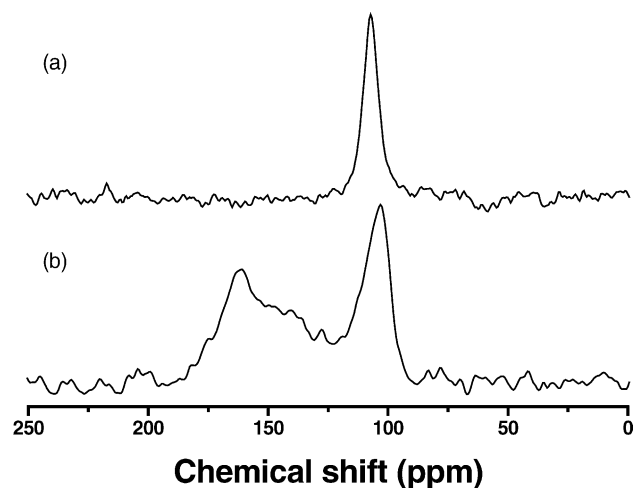

Fig. 6. Room-temperature ^{129}Xe NMR spectra of Xe (loading 1 amagat) co-adsorbed with 1,3,5-TMB on parent MCM-22 zeolite: (a) before; and (b) after sample heat treatment at 473 K for 3 d.

organic adsorbates in the intracrystalline voids of the zeolite adsorbent. This is not observed after thermal treatment (473 K for 3 d), in which the 1,3,5-TMB molecules eventually migrate into the intracrystalline voids of the sample, as evidenced by the [129]Xe NMR spectrum in Fig. 6b. Additional experiments performed on the same sample using solid-state ^{13}C NMR further verify this point (not shown). It can be seen that, after the thermal treatment, the [129]Xe NMR spectrum obtained from MCM-22 co-adsorbed with 1,3,5-TMB and Xe (loading 1 amagat) reveals three resonance peaks at ca. 103, 142 and 160 ppm. The spectrum is somewhat analogous to that obtained from MCM-22 at low temperature, except for the higher observed chemical shifts (due to an additional contribution from Xe-TMB interactions) and notable suppression of the peak at ca. 103 ppm, which has been ascribed previously to Xe in supercages. Note that, owing to its size, 1,3,5-TMB can be accommodated only in the supercages but not in the 10-MR channels. Thus, suppression of the peak at lower chemical shift can be explained by the presence of approximately one 1,3,5-TMB molecule in each supercage, which in turn reduces the effective free volume of the voids and thus results in a lower Xe adsorption. Consequently, the other two peaks can be assigned due to Xe adsorbed in the 10-MR channels.

3.4. Location and dispersion of Mo species

It has been shown that, for xMoOM22IC samples ($x = 2$–10), the Xe adsorption capacity tends to decrease with increasing Mo loading, especially when $x < 6$ wt.%, but remains practically unchanged for $x \geq 6$ wt.%. On the other hand, it has been shown that the slope (σ_{Xe}) of the $\delta(\rho)$ versus ρ plot (Fig. 3) in the low Xe loading regime should be inversely proportional to the effective free volume of the intracrystalline voids in zeolite [23,27]. That is:

$$\frac{V}{V_o} = \frac{(\sigma)}{(\sigma)_{Mo}} \tag{4}$$

where V and V_o represent the effective free volume of Mo/MCM-22 and the parent MCM-22 sample, respectively. Accordingly, the V/V_o ratios obtained from various samples are depicted in Table 1. A consistent decrease in V/V_o value with increasing Mo loading for $x < 6$ wt.% is evident. However, upon reaching a Mo loading level of 6 wt.%, the V/V_o ratios reach a plateau value of ca. 75% regardless of further increase in Mo loading. The results deduced from the aforementioned [129]Xe NMR parameters are therefore, in agreement with the Xe adsorption studies, suggesting that Mo species tend to deposit in the intracrystalline micropores of MCM-22 zeolite when $x < 6$ wt.%, but prefer to locate at the extracrystalline voids when $x > 6$ wt.%. In this context, the excessive Mo species are most likely to anchor either near the pore-mouths of the 10-MR channels or on the side-pockets existing on the extracrystalline surface of Mo/MCM-22. As such, owing to the extremely large macropores

between the zeolite crystallites, Xe atoms behave more like free gas and hence [129]Xe nuclei are relatively insensitive in probing changes in local environments on the external surface. That the δ_s and λ (or effective pore diameter) values remain unchanged for xMoOM22IC with $2 < x \leq 6$ wt.%, and that the former increases and the latter decreases with increasing Mo loading > 6 wt.%, provides additional support to the above notion. In addition, the fact that the observed V/V_o ratios remain practically unchanged also indicates that Mo species may be highly dispersed and nearly no MoO_3 exists as bulk phase. In contrast, at low Mo loadings < 6 wt.%, the amount of Mo species may be insufficient to disperse evenly in the intracrystalline void of Mo/MCM-22, thus leading to the broadening and splitting of the [129]Xe NMR resonance, as evidenced by the spectra obtained at lower temperature (Fig. 5b) between 180 and 220 K.

Similarly, the effects of different preparation procedures on porosity and location of Mo species can also be inferred from the [129]Xe NMR parameters listed in Table 1. By comparing the σ_{Xe} (or V/V_o) values obtained from various samples loaded with 6 wt.% Mo, it is clear that, in terms of ensuring incorporation of Mo species into the intracrystalline voids of Mo/MCM-22 zeolite, samples prepared by the impregnation method with additional calcination are more superior to samples prepared by physical mixing and/or samples without the thermal treatment. Moreover, for samples prepared by mechanical mixing, those mixed with Mo_2C appear to be more feasible than those with MoO_3. Again, these conclusions are consistent with the results obtained by Xe adsorption studies. It is also intriguing to find that thermal treatment has only marginal effect for samples prepared by physical mixing with Mo_2C, as can be seen by comparing the [129]Xe NMR parameters obtained from 6MoCM22M and 6MoCM22MH (Table 1). The fact that the δ_s values obtained from samples prepared by mechanical mixing and those without thermal treatment are in general greater than xMoOM22IC samples, also indicates that the chemical contribution arising from interactions between Xe and Mo species is less for the latter. In other words, samples prepared by physical mixing and/or samples without thermal treatment tend to result in bulkier Mo species that disperse inhomogeneously in Mo/MCM-22.

3.5. Acidity characterization by ^{31}P MAS-NMR of adsorbed TMPO

Fig. 7 displays the ^{31}P MAS-NMR spectra of TMPO adsorbed on MCM-22 and various xMoOM22IC samples. Detailed analyses by the Gaussian deconvolution method revealed that as many as 10 different resonance peaks, spanning a chemical range of 31.4–83.0 ppm, may be resolved from the spectrum obtained from the parent MCM-22 sample. The two peaks with lowest chemical shifts of 41.3 and 31.4 ppm can be unambiguously assigned as due to physisorbed TMPO [16,21]. Unlike the other peaks,
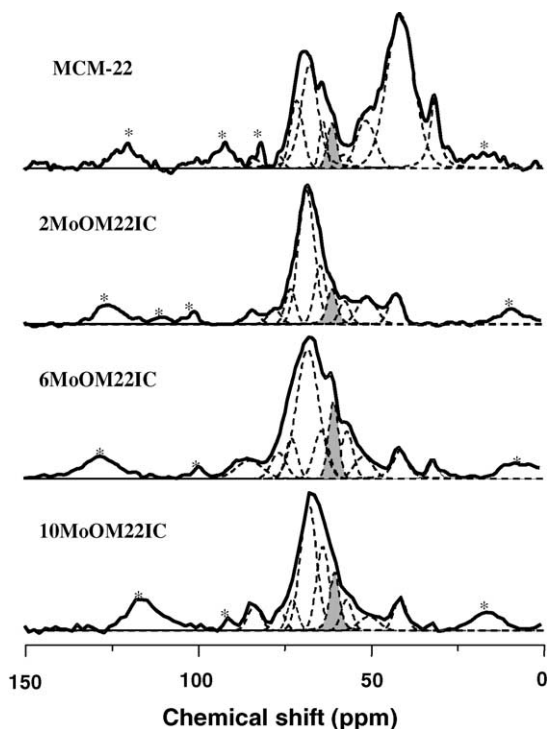
Fig. 7. Solid-state ^{31}P MAS-NMR spectra of TMPO adsorbed on parent MCM-22 and various calcined xMoOM22IC samples (x = 2–10 wt.%) prepared by the impregnation method. The dashed lines represent Gaussian simulation results. The shaded peaks denote resonance arising from TMPO adsorbed on Lewis acid sites. Typically, a sample spinning rate of 10–12 kHz was used.

which arise from TMPO adsorbed on Brønsted or Lewis acid sites, the contributions from the two physisorbed TMPO are irrelevant in terms of acidic features of the catalyst and thus are discarded in Table 2. Furthermore, by incorporating the results obtained from elemental analyses by ICP, concentra-

tions of acid sites in each sample can be determined, as also depicted in Table 2. The detailed analysis procedure invoked can be found elsewhere [21].

In an earlier study [28], it has been confirmed that the peak at 60.9 ppm is due to TMPO adsorbed on Lewis acid sites. This assignment was made possible by comparing the relative peak intensities of the resonance when the sample is subjected to various degrees of hydration treatments. With the exception of the peak at 60.9 ppm, the rest of the (7) peaks listed in Table 2 are provoked by interactions between the partially negative-charged oxygen atoms on TMPO adsorbate and the bridging hydroxyls (Brønsted acid sites) in MCM-22 zeolite. As the result, O–H chemical bonds are formed [16]. Consequently, the density of the electron cloud surrounding the ^{31}P nucleus neighboring the oxygen atom on TMPO should decrease with increasing acid strength of the Brønsted acid sites, which in turn causes the ^{31}P resonance to shift towards lower field. Thus, the resonance peak with higher chemical shift would reflect the Brønsted acid site having a stronger acidic strength [21]. Osegovic and Drago derived an empirical relation between the acid strength and the ^{31}P chemical shift (δ) of TMPO [29]:

$$-\Delta H = \frac{\delta - 34.892}{0.95 \times 4.1868} \text{ kJ/mole} \qquad (5)$$

where $-\Delta H$ represents the adsorption energy of the acid site measured by calorimetric titration with pyridine. Accordingly, the adsorption energy for each acid site for each sample can be estimated, as also depicted in Table 2. For comparison, acid sites with different acidic strengths can roughly be categorized into three groups [30], namely: (i) strong acidity with $-\Delta H \geq 150$ kJ/mole or $\delta \geq 70$ ppm; (ii) medium acidity with $100 < -\Delta H < 150$ kJ/mole or $58 < \delta < 70$ ppm; and (iii) weak acidity with $-\Delta H \leq 100$ kJ/mole or δ

Table 2

Assignments of ^{31}P NMR chemical shift and corresponding adsorption energy and distribution of acid sites for various samples[abc]

Sample	Chemical shift/$-\Delta H$/acid concentration								Total acidity[d]
MCM-22	**83.0**	**75.8**	**71.1**	**67.4**	**63.5**	**60.9**[e]	**57.5**	**51.2**	
	212	*180*	*159*	*143*	*126*	*114*	*100*	*72*	
	(0.009)	(0.009)	(0.088)	(0.212)	(0.034)	(0.440)	(0.017)	(0.092)	(0.470)
2MoOM22IC	**84.0**	**77.6**	**72.9**	**68.3**	**64.3**	**60.9**[e]	**57.2**	**50.7**	
	216	*188*	*167*	*147*	*129*	*114*	*98*	*70*	
	(0.012)	(0.012)	(0.024)	(0.136)	(0.044)	(0.025)	(0.019)	(0.031)	(0.278)
6MoOM22IC	**85.0**	**76.5**	**72.8**	**68.1**	**64.1**	**60.6**[e]	**56.7**	**51.9**	
	220	*183*	*167*	*146*	*129*	*113*	*96*	*75*	
	(0.021)	(0.018)	(0.020)	(0.127)	(0.031)	(0.034)	(0.028)	(0.018)	(0.263)
10MoOM22IC	**84.0**	**76.8**	**73.0**	**68.3**	**64.1**	**60.7**[e]	**57.2**	**50.7**	
	216	*184*	*168*	*147*	*129*	*114*	*98*	*70*	
	(0.014)	(0.010)	(0.014)	(0.088)	(0.046)	(0.028)	(0.019)	(0.012)	(0.203)

[a] For each sample, data in upper row (in **boldface**) denote the observed ^{31}P NMR chemical shifts (in ppm). Resonance peaks with chemical shift lower than 50 ppm (see Fig. 7), which arise from physisorbed TMPO, are excluded. For comparison, results obtained from various samples representing TMPO adsorbed on Brønsted (or Lewis) acid sites with practically the same acidic strengths are aligned in the same column.

[b] Data in middle row (in italics) denote the estimated adsorption energy (in kJ/mole) derived from Eq. (5).

[c] Data in lower row (in parentheses) denote acid concentration ($\pm$ 0.002 mmole/g cat.) of the corresponding acid site.

[d] Total concentration of Brønsted acid sites (in mmole/g cat.).

[e] Data in shaded column denote resonance arising from TMPO adsorbed on Lewis acid sites.

$\leq$ 58 ppm. The average adsorption energies of these three groups, as estimated by a weighted average of their relative acid concentrations, are found to be 165, 124 and 76 kJ/mole, respectively. In terms of acid distributions, ca. 12, 75 and 13% of the total acidity, respectively arises from the strong, medium and weak acidity. Nevertheless, it is noted that the observed ^{31}P NMR chemical shifts, which reflect changes at the local environments surrounding the ^{31}P nucleus in the probe molecule, should be much more sensitive to the strength of acid sites compared to typical analytical methods and hence should be more advantageous in terms of discernment and quantification of acid sites.

Upon loading of Mo < 6 wt.%, a slight increase (ca. 1 ppm) in chemical shift of each respective peak can be observed, especially for those corresponding to acid sites with higher acid strengths. This suggests a slight increase in the overall acidic strength of MCM-22 upon Mo incorporation. Regardless of this small difference in chemical shift, assignments of various acid sites with specific acidic strength (i.e., having roughly the same chemical shift) should remain valid. Further combining the ^{31}P NMR results with data obtained from elemental analyses by ICP provides a determination of acid concentration [21]. The results are also shown in Table 2.

It is worth noting that the acid concentration so determined is somewhat different from the Al concentration, which should have a 1:1 correspondence with the Brønsted acid site. For example, in parent MCM-22, the total acid concentration is ca. 0.47 mmole/g; a value much smaller than the Al concentration (ca. 1.04 mmole/g) can be inferred. Omission of the acid sites located in the 10-MR channels of MCM-22, whose high tortuosity and limited pore diameter are inaccessible to TMPO, should be responsible for the discrepancy observed. Nevertheless, since our main objective is to determine the effect of Mo incorporation on variation of acid sites in MCM-22, in which the Mo species were found to locate mostly in the larger supercages (see above), the acid concentrations obtained from samples with various Mo loading (Table 2) should still be useful. Consequently, a total Brønsted acidity of 0.470, 0.278, 0.263, and 0.203 mmole/g is found for MCM-22, 2MoO-M22IC, 6MoOM22IC and 10MoOM22IC, respectively. A drastic decrease in both Brønsted and Lewis acidity immediate upon incorporation of Mo species into MCM-22 is therefore evident. For example, a respective decrease of ca. 41% and 94% in total Brønsted and Lewis acidity was found for 2MoOM22IC compared to parent MCM-22. However, only marginal decreases were observed when the Mo loading was increased from 2 to 6 wt.%. As the Mo loading is increased to 10 wt.%, further decrease in total acid concentration is noticeable. It is also noted that the amounts of acid sites with highest acidic strengths (at chemical shift ca. 84 and 76 ppm) seem to increase at the expanse of weaker acidity while increasing Mo loading, reaching a highest value at ca. 6 wt.% loading then decreasing accordingly when Mo loading is further increased.

By comparing the catalytic performances of various Mo/MCM-22 catalysts with varied Mo loading from 2–10 wt.% reported by Bao and co-workers [4], they concluded that an optimal performance can be achieved by catalyst having a Mo loading of 6 wt.%, namely with depressed naphthalene yield and prolonged catalyst life. More specifically, for Mo/MCM-22 catalysts with Mo loading of 2, 6 and 10 wt.%, a methane conversion of 5.7, 10, and 5.8 % and a benzene selectivity of 67.8, 80.0 and 61.4 % were respectively, determined. A similar trend is also observed in this study for the variations in the concentrations of both Brønsted and Lewis acid sites. Thus, the results obtained from this study imply that while both types of acidity may be responsible for catalyzing the methane dehydroaromatization reaction over Mo/MCM-22, Brønsted acid sites with high acidic strengths should play the dominant role.

4. Conclusions

The porosity and acidity features of Mo/HMCM-22 catalysts prepared by different methods and with varied Mo loading have been examined by [129]Xe and ^{31}P MAS-NMR techniques using suitable adsorbed probe molecules, namely Xe and TMPO, together with Xe adsorption measurements and elemental analyses by ICP.

The results obtained from variable-temperature [129]Xe NMR of Xe adsorbed on parent MCM-22 revealed three distinct environments. Among them, the two resonance peaks having higher chemical shifts are responsible for Xe adsorbed in the 10-MR channels, whereas the other peak with lower chemical shift is due to Xe in supercages in which Xe is more preferably adsorbed. It is found that, in terms of competency of incorporating Mo species into the intracrystalline voids of MCM-22, sample preparation by mechanical mixing is less favorable than by the impregnation method. Moreover, sample calcination treatment is essential in ensuring a well-dispersed Mo species in Mo/MCM-22. Moreover, upon initial incorporation, drastic decreases in both total Brønsted and Lewis acidities were observed. For the former, Mo species preferably deactivate weaker acid sites in the supercages rather than in the 10-MR channels of MCM-22. However, as the Mo loading exceeds 6 wt.%, the excessive Mo species tend to deposit either near the pore-mouths of the 10-MR channels or reside in the side-pockets on the extracrystalline surfaces of the catalyst.

Furthermore, for samples prepared by the impregnation method, slight increases in concentrations for acid sites with highest acid strengths with increasing Mo loading (<6 wt.%), at the expense of weaker acid sites, are evident. On the other hand, further increase in Mo loading > 6 wt.% results in further decrease in both Brønsted and Lewis acidities. In any case, a slight increase in the overall acidic strength is accompanied by a noticeable decrease in total acidity upon loading of Mo species onto MCM-22. Together with the results obtained from [129]Xe NMR studies, this

indicates that Mo species, which preferably locate in the supercages at low coverage, tend to deactivate acid sites in MCM-22 zeolite and in the meantime also slightly modify the catalyst to result in a slight increase in its overall acidic strength.

The results obtained from this study therefore, provide prominent support in explaining the unique catalytic performances observed earlier during the methane dehydroaromatization reaction over Mo/MCM-22 catalyst with a peculiar Mo loading of 6 wt.%. It is concluded, that both Brønsted and Lewis sites may be responsible for catalyzing the methane conversion reaction. Furthermore, in terms of Brønsted acidity, acid sites with higher acid strengths are more likely to play a dominant role.

Acknowledgements

Reference

[1] S. Wong, Y. Xu, W. Liu, L. Wang, X. Guo, Appl. Catal. A 136 (1996) 7.
[2] B.M. Weckhuysen, D. Wang, M.P. Rosynek, J.H. Lunsford, J. Catal. 175 (1998) 338.
[3] Y. Xu, L. Lin, Appl. Catal. A 188 (1999) 53.
[4] Y. Shu, D. Ma, L. Xu, Y. Xu, X. Bao, Catal. Lett. 70 (2000) 67.
[5] M.K. Rubin, P. Chu, US Patent 4954325 (1988).
[6] T. Yashima, K. Miura, T. Komatsu, Zeolites Rel. Microporous Mater. 84 (1994) 1897.
[7] T. Ito, J. Fraissard, J. Phys. Chem. 76 (1982) 5225.
[8] J.A. Ripmeester, J. Am. Chem. Soc. 104 (1982) 289.
[9] J.L. Bonardet, J. Fraissard, A. Gedeon, M.A. Springuel-Huet, Catal. Rev. -Sci. Eng. 41 (1999) 115.
[10] C.I. Ratcliffe, Annu Rep. Nucl. Magn. Reson. Spectrosc. 36 (1998) 124.
[11] F. Chen, F. Deng, M. Cheng, Y. Yue, C. Ye, X. Bao, J. Phys. Chem. B 105 (2001) 9426.
[12] J.H. Lunsford, W.P. Rothwell, W. Shen, J. Am. Chem. Soc. 107 (1985) 1540.
[13] J.H. Lunsford, Top. Catal. 4 (1997) 91.
[14] B. Zhao, H. Pan, J.H. Lunsford, Langmuir 15 (1999) 2761.
[15] H.M. Kao, C.Y. Yu, M.C. Yeh, Microporous Mesoporous Mater. 53 (2002) 1.
[16] E.F. Rakiewicz, A.W. Peters, R.F. Wormsbecher, K.J. Sutovich, K.T. Mueller, J. Phys. Chem. B 102 (1998) 2890.
[17] K.J. Sutovich, A.W. Peter, E.F. Rakiewicz, R.F. Wormsbecher, S.M. Mattingly, K.T. Mueller, J. Catal. 183 (1999) 155.
[18] Q. Zhao, W.H. Chen, S.J. Huang, Y.C. Wu, H.K. Lee, S.B. Liu, Stud. Surf. Sci. Catal. 141 (2002) 453.
[19] L. Baltusis, J.S. Frye, G.E. Maciel, J. Am. Chem. Soc. 108 (1986) 7119.
[20] L. Baltusis, J.S. Frye, G.E. Maciel, J. Am. Chem. Soc. 109 (1987) 40.
[21] Q. Zhao, W.H. Chen, S.J. Huang, Y.C. Wu, H.K. Lee, S.B. Liu, J. Phys. Chem. B 106 (2002) 4462.
[22] L.S. Lee, S.T. Oyama, M. Boudart, J. Catal. 106 (1987) 125.
[23] S.B. Liu, S. Prasad, J.F. Wu, L.J. Ma, T.C. Yang, J.T. Chiou, J.Y. Chang, T.C. Tsai, Appl. Catal. A 159 (1993) 664.
[24] W.H. Chen, A.R. Pradhan, S.J. Jong, T.Y. Lee, I. Wang, T.C. Tsai, S.B. Liu, J. Catal. 163 (1996) 436.
[25] S.J. Jong, J.F. Wu, A.R. Pradhan, H.P. Lin, C.Y. Mou, S.B. Liu, Stud. Surf. Sci. Catal. 117 (1998) 543.
[26] J. Demarquay, J. Fraissard, Chem. Phys. Lett. 136 (1987) 314.
[27] J. Fraissard, T. Ito, Zeolites 8 (1988) 350.
[28] Q. Zhao, S.J. Huang, W.H. Chen, S.B. Liu, Stud. Surf. Sci. Catal. 145 (2003) 205.
[29] J.P. Osegovic, R.S. Drago, J. Phys. Chem. B 104 (2000) 147.
[30] D. Meloni, S. Laforge, D. Martin, M. Guisnet, E. Rombi, V. Solinas, Appl. Catal. A 215 (2001) 55.